



Revealing the Specific Spatial Confinement in 8-membered Ring Cage-type Molecular Sieves via Solid-state NMR and **Theoretical Calculations**

Caiyi Lou, [a, b] Wenna Zhang, [a] Chao Ma, [a, b, c] Benhan Fan, [a, b] Shutao Xu, *[a] Shushu Gao, [a] Peng Guo, [a] Yingxu Wei, *[a] and Zhongmin Liu*[a, d]

Spatial confinement plays a significant role in selective adsorption and catalysis of molecular sieves. In this work, the adsorption behaviors of methanol in 8-membered ring cagetype molecular sieves DNL-6 and SAPO-42 were investigated by ¹³C solid-state NMR (ssNMR) and density functional theory (DFT) calculations. Confinement-induced spatial orientation of guest molecules in molecular sieves was revealed with considering both confined space and active centers. Confined space of double 8-membered rings (D8R) in DNL-6 favors the adsorption of methanol, accompanied by the methyl groups orientating to D8R space and the hydroxyl groups of methanol anchored by Brønsted acid site (BAS).

Molecular sieves have been widely applied in heterogeneous catalysis, gas adsorption and ion-exchange due to their finely adjustable pore size and acidity.[1-4] Adsorption, a prior step of the whole process of suface reactions, [5] is pivotal to gas-solid catalysis and may influence the reaction process and rates. Therefore, revealing the adsorption behavior is important to well understand the reaction mechanism and structure-performance relationship.

The adsorption properties are mainly dependent on the host-quest interaction between adsorbent molecules and framework. Besides the size and properties of guest molecules, the acidity and porosity of host molecular sieves will affect the adsorption and mass transfer processes. [6-11] Additionally, the distinction of acidity and confined environment may lead to the selective adsorption. To this regard, ssNMR is a powerful method to characterize the detailed acidity and the structure properties of molecular sieve, and it is capable of probing the host-guest interactions between adsorbed molecules and molecular sieve since the NMR chemical shift is rather environment-sensitive. [7,12-17] Moreover, theoretical calculations can be exploited as a versatile method to identify the NMR signals of confined species in molecular sieves and study the structure activity relationship.[18-20]

DNL-6, a 8-membered ring SAPO-based zeolite firstly reported by our group in 2011,[21] is RHO topology with bodycentered cubic symmetry structure ($Im\bar{3}m$, a = 14.9 Å) which is composed of large Ita cages interconnected, via short narrow D8R channels, in three dimension mode (shown in scheme 1a). Due to its strong acidity compared to some other SAPOs like SAPO-34 and special confined environment, DNL-6 has been

[a] C. Lou, Dr. W. Zhang, C. Ma, B. Fan, Prof. S. Xu, Dr. S. Gao, Dr. P. Guo, Prof. Y. Wei, Prof. Dr. Z. Liu National Engineering Laboratory for Methanol to Olefins Dalian National Laboratory for Clean Energy iChEM (Collaborative Innovation Center of Chemistry for Energy Materials) Dalian Institute of Chemical Physics Chinese Academy of Sciences Dalian 116023 (P. R. China) E-mail: xushutao@dicp.ac.cn weiyx@dicp.ac.cn liuzm@dicp.ac.cn [b] C. Lou, C. Ma, B. Fan

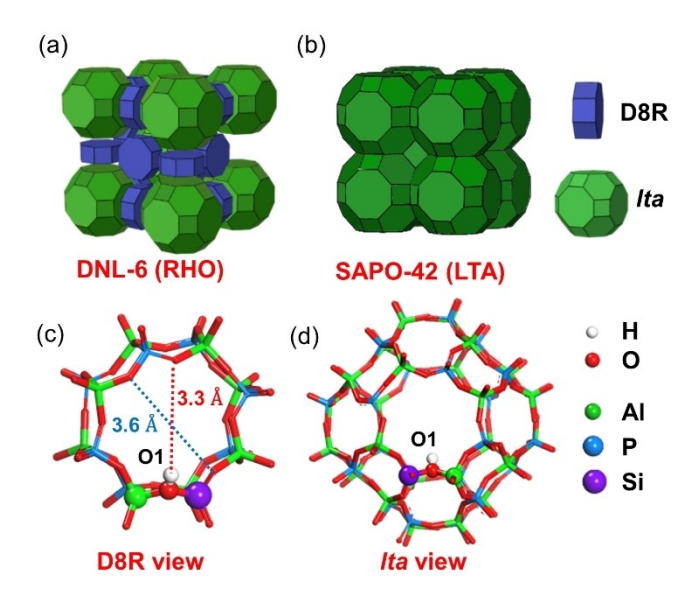
University of Chinese Academy of Sciences Beijing 100049 (P. R. China)

Zhang Dayu School of Chemistry Dalian University of Technology Dalian 116024 (P. R. China) [d] Prof. Dr. Z. Liu State Key Laboratory of Catalysis

Dalian Institute of Chemical Physics Chinese Academy of Sciences Dalian 116023 (P. R. China)

Supporting information for this article is available on the WWW under https://doi.org/10.1002/cctc.202001682

This publication is part of a Special Collection on "Catalysis in Confined Spaces". Please check the ChemCatChem homepage for more articles in the collection



Scheme 1. 3D models highlighted by dark green-filled Ita cages and navyfilled D8R structures of RHO (a) and LTA (b) topologies. (c) and (d) show the optimized structures of BAS (O1 site) lying between the D8R and Ita cavity seen from the D8R view (c) and Ita view (d), respectively.



applied in methanol to olefins (MTO) conversion and carbon dioxide adsorption.[22,23] In this work, DNL-6 was employed as the host to investigate the methanol adsorption behavior at room temperature. ¹³C NMR spectroscopy was applied to distinguish the methanol adsorption by correlating the local chemical surroundings of methyl groups to their chemical shifts. Methanol adsorption stability of different configurations was calculated to clarify the function of D8R and acid sites. Moreover, the host-guest interactions between the molecular sieve and methanol molecule were visualized via isosurface plots of reduced density gradient (RDG). Additionally, considering that the specific confined space (D8R) may make difference on the adsorption of methanol, SAPO-42 zeolite, with LTA topology also consisting of the Ita cavity while connected by a single 8-membered ring instead of D8R structure (shown in scheme 1b), was used as a comparison to dissect the detailed adsorption behavior imposed by confinement effect from D8R. Rather different from the inert molecules adsorbed in molecular sieves, methanol molecules adsorbed in the DNL-6 is through hydrogen-bond rather than merely simple van der Waals (vdW) forces (Scheme 1c, 1d showing BAS of O1 seen from the D8R and Ita view, respectively). [24-26] As most of the BASs occupied by methanol molecules, the protonated dimer or cluster complex of methanol would appear at high methanol loading and may influence the adsorption.[27]

The XRD and SEM results show that the DNL-6 and SAPO-42 samples are highly crystalline with size of ca. 2 μ m (Figure S1 and S2), and the 1 H MAS NMR spectra indicate that both

catalysts possess close amount of BASs (Figure S3). The loadingdependent ¹H MAS NMR spectra of ¹³CH₃OH adsorbed in DNL-6 and SAPO-42 are displayed in Figure S4 and S5, respectively. The ¹H NMR chemical shifts of hydroxyl resonances decrease with increasing the methanol coverage, which is probably caused by a rapid chemical exchange between hydroxyl protons of Brønsted acid and of methanol molecules.[25] Figure 1a and 1b exhibit the ¹³C MAS NMR spectra of methanol adsorbed in DNL-6 and SAPO-42, and the intensities of these two main signals enhance with increasing the feeding methanol amount over the two SAPO materials, respectively. The main peaks appeared at around 51 (for DNL-6) and 50 ppm (for SAPO-42) are assigned to the adsorbed methanol, and a rather weak peak located at 55~56 ppm for DNL-6 and SAPO-42 might be attributed to the surface methoxy species (SMS). [15,28, ^{29]} Detailed relationships between the adsorption concentration and the ¹³C NMR chemical shifts of methanol adsorbed in DNL-6 $(\delta_{\rm DNL\text{-}6})$ and SAPO-42 $(\delta_{\rm SAPO\text{-}42})$ are provided in Figure 1c. The $\delta_{\text{SAPO-42}}$ presents a monotonical increasement from 49.7 to 50.2 ppm as a function of adsorbate coverage from 0.83 to 5.72 per lta cage (Figure 1c black line). Differently, $\delta_{\text{DNL-6}}$ presents a parabolic-like trend (Figure 1c red line), and the value of chemical shift declines from 51.3 to 50.9 ppm as adsorption amount increased from 0.04 to 3.95 per Ita cage, then the peak position gradually shifts to the lower field with further increasing the ¹³CH₃OH coverage to 6.09 per *Ita* cage.

The chemical shift is dependent on the effective magnetic fields directly, and it is influenced by various interactions and

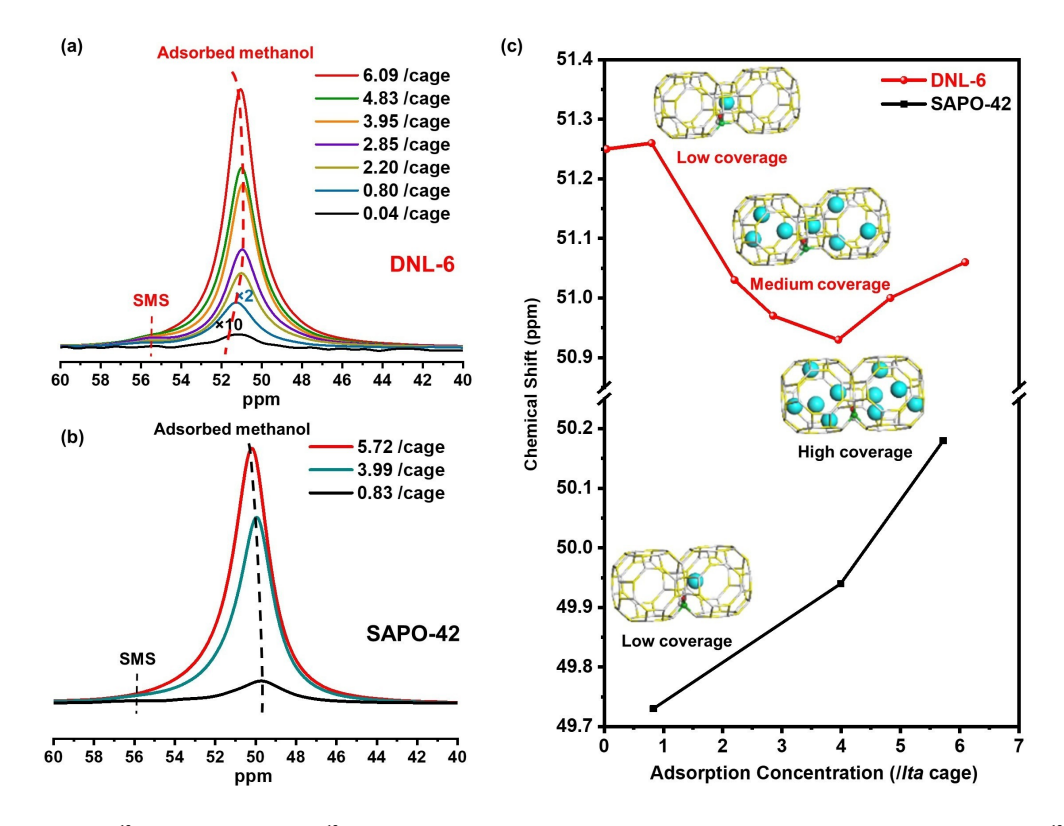


Figure 1. Loading-dependent ¹³C MAS NMR spectra of ¹³CH₃OH adsorbed in the DNL-6 (a) and SAPO-42 (b) zeolites at room temperature; (c) ¹³C chemical shifts of adsorbed methanol as a function of methanol molecules per *lta* cage (schematic drawing with the green balls representing the methanol molecules).



chemical environment. As mentioned above, methanol preferentially interacts with the molecular sieve by hydrogen-bond instead of simple physical adsorption, [24,25] and methanol molecules probably associate with each other to form protonated dimer or cluster complex of methanol at high concentration, owing to its limited number of BASS. [27] The BAS of the employed SAPO-42 has been proven to be located in site O1 by Rietveld Refinement in our previous work, by the usage of specific organic structure-directing agent (OSDA). [30,31] Thus, the single BAS and sole confined space of *Ita* provide exclusive adsorption site for methanol, and the increasing trend of the SAPO-42 is predominantly attributed to the interactions between adsorbate molecules, such as H-bonding interactions.

In the case of DNL-6, the variation of the $\delta_{ extsf{DNL-6}}$ shows a parabolic-like trend (Figure 1a and 1c). This goes against the trend in the case of singular adsorption site, which means that there are at least two kinds of situations for methanol adsorption corresponding to different BASs and confined environment. As well known, to get the maximal vdW attraction, the guest molecule is inclined to sit in the confined voids with comparable dimensions, achieving the best fit between organic molecule and inorganic environment.[8] Due to the distinction on structure between these two catalysts, a confinement effect stemmed from D8R structure needs to be illustrated explicitly. Generally, a more confined space, which provides a stronger host-quest interaction between absorbent molecules and molecular sieve framework, probably leads to a higher value of NMR chemical shift.[32] The D8R structure possesses more confined space than Ita cavity, obviously. The higher chemical shifts of resonances for DNL-6 indicate that methanol is probably prone to being adsorbed in D8R rather than Ita cavity (Figure 1c). Considering that the methanol molecule is adsorbed on the BAS by hydrogen bond interaction, [24,25] it is not simply located in D8R or Ita space. Hence, the more exact description may well be that the hydroxyl group of methanol is anchored by BAS with less freedom, while the methyl group is inclined to orientate to D8R space rather than *Ita* cage. In addition, there is probably a fast exchange of adsorbed methanol between D8R and Ita orientation due to the observed peaks are single and symmetrical, and the δ_{DNL-6} could be expressed as follow (Eq. (1)): [32]

$$\delta_{\text{DNL-6}} = P_{\text{D8R}} \delta_{\text{D8R}} + P_{\textit{lta}} \delta_{\textit{lta}} = P_{\text{D8R}} \delta_{\text{D8R}} + (1 - P_{\text{D8R}}) \delta_{\textit{lta}} \tag{1}$$

where $\delta_{\rm D8R}$ and $P_{\rm D8R}$, δ_{lta} and P_{lta} refer to the chemical shift and proportion of the methyl groups located at D8R space and lta cavity, respectively. For the limited number of D8R structures, with the increase of methanol loading, more and more methanol molecules have to be orientated in lta cage, which decreases the value of $P_{\rm D8R}$ and leads to the decline of $\delta_{\rm DNL-6}$ from 51.3 to 50.9 ppm. With the further increase of methanol loading, especially higher than 3.95 per cage, almost all of the D8R spaces are occupied and more molecules are crowded into lta cavities. For the enhanced interactions between methanol molecules, such as H-bonding interactions, it results in gradually ascending of the $\delta_{\rm DNL-6}$, similar to that in SAPO-42.

Besides the influence of the space confinement, different acid sites can also make difference on the chemical shift of guest molecules.^[7,13,33,34] To further reveal the detailed information of the methanol adsorption behavior, theoretical calculation from a microscopic point of view was employed. DNL-6 molecular sieve contains two kinds of BASs, because of two non-equivalent oxygen sites located at different intersection positions of rings (acid site O1 surrounded by 4, 6, 8-membered rings (MR) and O2 with 4, 4, 8-MR, respectively), which are all presented in the junction of two confined spaces originating from D8R and Ita cage Therefore, considering the methanol orientation, four kinds of adsorption configurations including two confined structures with two kinds of acid sites were modelled. As displayed in Figure 2, configurations a and c show the hydroxyl anchored on the acid site O1 with the methyl group orientating to D8R space and Ita cage, respectively, while b and d exhibit the methanol adsorbed on the site O2 with D8R and *Ita* orientation, respectively. Adsorption energies (ΔE_{ads}) were calculated to evaluate the stability of methanol adsorbed on various acid sites and different confined spaces, and it could be defined (Eq. (2)):

$$\Delta E_{\text{ads}} = E_{\text{methanol-HZ}} - E_{\text{HZ}} - E_{\text{methanol}} \tag{2}$$

where $E_{\text{methanol-HZ}}$ is the total energy of the zeolite complex when methanol is adsorbed on the BAS, and E_{HZ} and $E_{methanol}$ stand for the energies of the isolated zeolite host and free methanol molecule guest, respectively. As shown in Figure 2, the adsorption energies of acid site O1 (-125.0 and -119.7 kJ mol $^{-1}$ for D8R orientation and Ita orientation) are slightly lower by $2.4-3.3 \text{ kJ} \text{mol}^{-1}$ than that on site O2 -121.7 and $-117.3 \text{ kJ} \, \text{mol}^{-1}$ for D8R orientation and *lta* orientation), suggesting methanol molecules prefer to being adsorbed on the acid site O1, which is ascribed to their acidity that can be evaluated by the deprotonation energy (DPE).[35,36] A smaller DPE value represents a stronger Brønsted acidity. The calculated DPE value of acid site O1 is 1177.4 kJ mol⁻¹ lower by about 13 kJ mol⁻¹ than that of site O2 (1190.3 kJ mol⁻¹) in these models, illustrating the acid site O1 possesses relative stronger acidity. Nevertheless, it is obviously found that the D8R confined space plays a more significant role in stabilizing the methanol adsorption, since the methanol molecule toward to D8R orientation exhibits lower adsorption energy by 4.4- 5.3 kJmol^{-1} (5.3 kJmol⁻¹ for O1 and 4.4 kJmol⁻¹ for O2) than that toward to Ita cavity. These results prove that D8R space matches well with the adsorption molecule, and the distinction of stability is predominantly caused by confined space rather than acidity.

Furthermore, the calculated ¹³C NMR chemical shifts of adsorbed methanol further prove the special confinement of D8R structure. As presented in Figure 2. the chemical shifts of methanol with *Ita* orientation in DNL-6 (51.4 and 51.2 ppm for site O1 and O2) are similar to that adsorbed in the *Ita* cavity of SAPO-42 (51.6 ppm), and the chemical shifts of D8R orientation (52.1 and 52.4 ppm for O1 and O2) are about 1.0 ppm higher than that of *Ita* orientation, which coincides with the ¹³C NMR experiment. Nevertheless, lower adsorption energies (the stron-



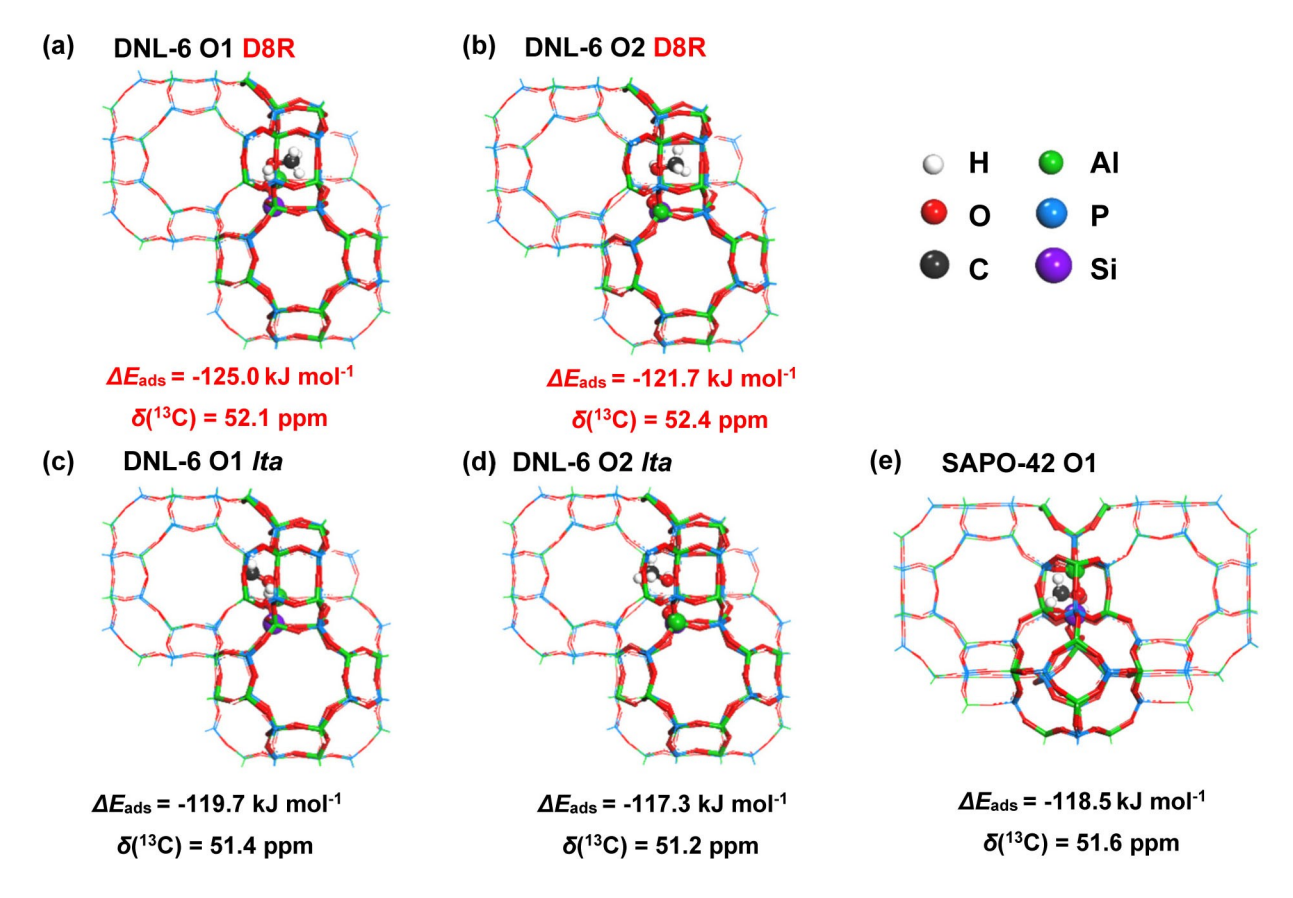


Figure 2. Optimized geometries of the methanol adsorbed DNL-6 (a-d) and SAPO-42 zeolites (e): (a) adsorbed on O1 site with D8R orientation, (b) adsorbed on O2 site with D8R orientation, (c) adsorbed on O1 site with Ita cage orientation, (d) adsorbed on O2 site with Ita cage orientation, (e) adsorbed on the O1 site of SAPO-42 (the O1 location has been proven by Rietveld Refinement).

ger interaction) of methanol with D8R orientation illustrate that the methyl group is inclined to D8R space prior to Ita cage, leading to a high $\delta_{\text{DNL-6}}$ value in the case of low methanol coverage. With increasing of the methanol adsorption amount, since the larger Ita cavity can adsorb more methanol molecules than D8R space, a larger proportion of methanol molecules turns to orientate to or is directly located in the Ita cages, resulting in a lower δ_{DNL-6} value. As the methanol adsorption amount is above 3.95 per cage, similar to SAPO-42, the δ_{DNL-6} moves to a lower field, owing to the enhanced interactions between methanol adsorbate molecules.

To further visualize the interaction between the molecular sieve framework and the adsorbed molecule, the isosurface plots of reduced density gradient for the adsorption configurations of D8R orientation (a) and Ita orientation (b) in the DNL-6 (acid site O1) are provided in Figure 3. The gradient isosurfaces enclosing the corresponding regions of real space could reflect the weak interaction between methanol molecule and molecular sieve framework. The isosurface of the methanol with Ita orientation exhibits a scattered distribution (Figure 3b). On the contrary, for the D8R orientation, the methanol molecule is surrounded by a large green area of isosurface in three-dimensional space. It is suggested that the adsorption configuration of D8R orientation displays stronger vdW interaction between the methanol and zeolite

www.chemcatchem.org

framework. The unique confinement imposed by the D8R structure and the stronger vdW interaction determines the methyl groups orientation and the higher stability of methanol molecules adsorption.

In summary, ¹³C NMR spectroscopy reveals the different adsorption orientations of methanol in DNL-6 molecular sieve at room temperature and suggests that D8R confined space facilitates the adsorption of methanol molecules. The adsorption orientations of methanol molecules presented by the experiments and theoretical calculation interpret the confinement effect from D8R chemical environment for guest molecule adsorption from a microscopic point of view. The specific confined effect makes differences on the adsorption behavior, which may directly influence the adsorption performance and mass transfer. Furthermore, it may influence the activation and conversion over different reaction centers and give rise to the distinct catalytic performances.

Experimental Section

Sample Preparation

The DNL-6 molecular sieve used in the adsorption experiments was synthesized by the conventional hydrothermal method. The gel



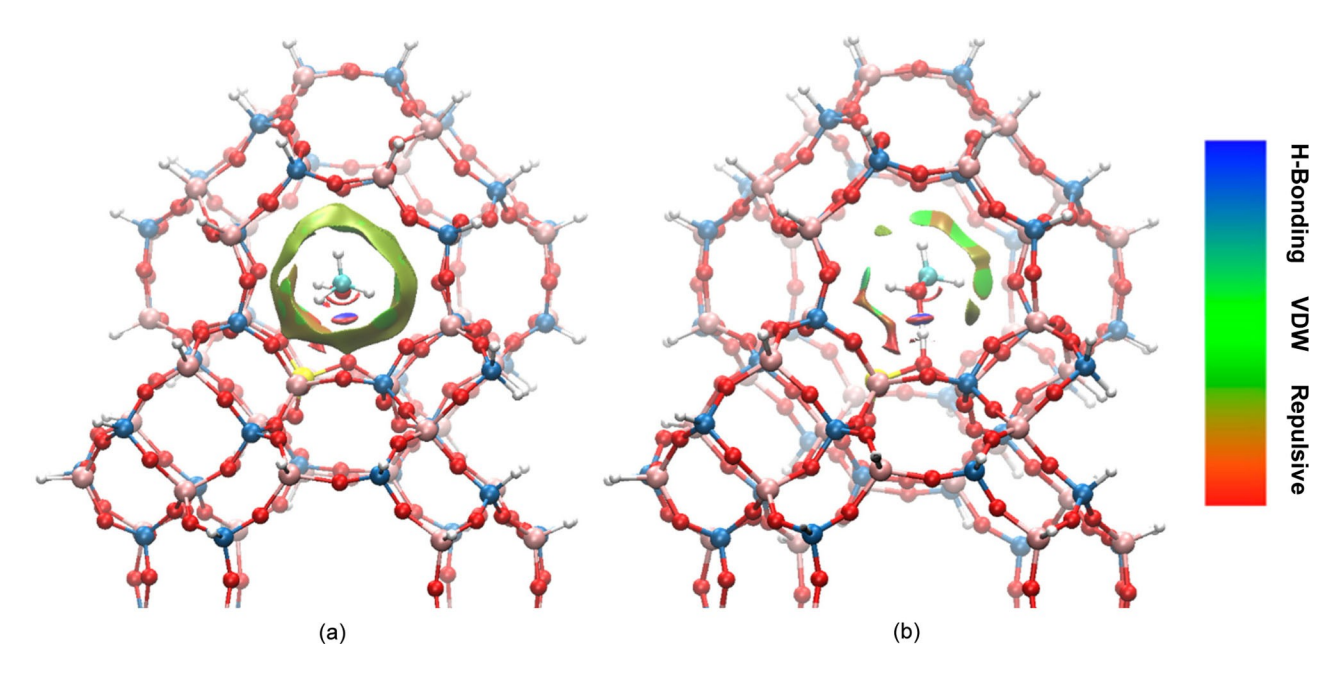


Figure 3. Isosurface plots of reduced density gradient for the adsorption configurations of D8R orientation (a) and Ita orientation (b).

composition is 1.0 DEA: 0.2 $SiO_2:0.4\ P_2O_5:0.5\ Al_2O_3:50\ H_2O:0.15\ CTAB.^{[37]}$ In the specific experiment, Orthophosphoric acid (85 wt.%), aluminum isopropoxide and deionized water were mixed and stirred vigorously. Then, the mixed solution with tetraethyl orthosilicate and diethylamine (DEA) was added dropwise into previous solution. After stirring several hours, cetyltrimethylammonium bromide (CTAB) was added into the above mixture. Stirring was kept during all the above mixing procedure. Finally, the gel mixture was transferred into Teflon-lined autoclaves and crystallized at 200 °C for 24 h under rotated conditions. The product was recovered by centrifuging, washing with deionized water repeatedly, and drying at 120 °C overnight. Calcination was carried out at 550 °C for 6 h to remove organic species.

Well-crystallized SAPO-42 sample was obtained with the gel composition of 2.0 DPA:0.35 SiO₂: 0.4 P₂O₅: 0.5 Al₂O₃: 50 H₂O: 0.15 CTAB: 10% seed (the amount of seed addition is based on the weight of Al₂O₃ in the synthesis system). Aluminum isopropoxide, phosphoric acid, and deionized water were mixed and stirred vigorously. Then tetraethyl orthosilicate and dipropylamine (DPA) were added sequentially. After stirring several hours, CTAB and a small amount of SAPO-42 seed were added. Then homogeneous gel was transported into Teflon-lined autoclaves and crystallized at 200°C for 24 h under the rotation state of 75 rmin⁻¹. The final products were recovered by centrifugation, washed with distilled water repeatedly, and dried at 120°C overnight. Calcination was carried out at 600°C for 4 h to remove organic species.

Adsorption of ¹³CH₃OH

Before the adsorption of methanol, calcined samples with known mass were dehydrated on a vacuum line at $420\,^{\circ}\text{C}$ for 16 h. Typically, the final pressure of vacuum line system will reach lower than $5.0\times10^{-4}\,\text{Pa}$ in order to remove water and other adsorbates. Following complete dehydration, an aliquot of $^{13}\text{CH}_3\text{OH}$ (the abundance of ^{13}C is 99%), with a known volume of vapor at a known operative temperature and pressure, was transferred into the adsorption tube. And then the valve of the tube was closed,

and the sample was equilibrated at room temperature for at least 1 h. Finally, the valve of the tube was opened to pump off the weak adsorption adsorbate for half an hour at room temperature, and the sample was transferred into 4 mm rotor in Ar protected glove box.

Characterization

The powder X-ray diffraction (XRD) patterns for phase identification were recorded on a PANalytical X' Pert PRO X-ray diffractometer in the range of $2\theta = 5-50^{\circ}$ with Cu–K α radiation ($\lambda = 1.5418$ Å). The crystal morphology was observed using field emission scanning electron microscopy (SEM) (Hitachi SU 8020 and TM3000). MAS NMR experiments were performed on a Bruker Avance III 600 spectrometer equipped with 14.1T wide-bore magnet. The spinning rates of 1 H, 13 C, 27 Al and 31 P spectra were 12 kHz, and that of 29 Si was 8 kHz, and the 13 C, 29 Si and 31 P MAS NMR spectra were recorded with a high-power proton decoupling sequence. The chemical shifts of 1 H, 13 C, 27 Al, 29 Si and 31 P spectra were respectively referenced to adamantane (1.74 ppm), hexamethylbenzene (with the upfield methyl peak at 17.35 ppm), Al(NO₃)₃ solution (0 ppm), kaolinite (-91.5 ppm) and (NH₄)₂HPO₄ (1.13 ppm).

Theoretical calculation

Computational Methods

For theoretical calculations, cluster models of 102T and 108T extracted from the crystallographic RHO and LTA structures were used to represent DNL-6 (Figure S6) and SAPO-42 (Figure S7), respectively. The terminal Si–O bond was treated by hydrogen atoms saturating. The geometries of methanol adsorption were predicted by combined theoretical ONIOM method, [38] and the methanol molecule, acid site and the parts interested (including D8R and the atoms around the



acid center) were set as high layer and treated with the density functional theory method, while the other atoms located in the environmental layer were regarded as low layer and treated with the semiempirical calculation method. The ωB97XD hybrid density function with 6-31G (d, p) basis sets and semi-empirical AM1 were employed for optimizing the structures of the high-level and low-level layer, respectively. The single-point energies were calculated at the level of $\omega B97XD/6-31G(d, p)$ on the basis of optimized structures. $^{[39,40]}$ Chemical shifts of the $^{13}\text{CH}_3\text{OH}$ adsorption complexes were calculated with B3LYP method in DGDZVP level and referenced to 17.35 ppm of Hexamethylbenzene (HMB) for the experimental value. And all the calculations were carried out with the Gaussian09 package.[41]

Interaction visualization

The noncovalent interaction index approach, [42] which provides a rich representation of van der Waals interactions, hydrogen bonds, and steric repulsion, was adopted to visualize the interactions between the host zeolite framework and guest methanol molecules. The reduced density gradient (RDG, defined as $s = 1/(2(3\pi^2)^{1/3}) |\nabla \rho|/(\rho^{4/3})$ and electron density (ρ) was employed to distinguish the covalent and noncovalent interactions. The regions with low density and low RDG represent noncovalent interactions, and the function $sign(\lambda_2)\rho$ represents different types of noncovalent interactions, i.e., sign $(\lambda_2)\rho < 0$, H-bonding interaction; $sign(\lambda_2)\rho \approx 0$, weak vdW interaction; and sign(λ_2) $\rho > 0$, strong repulsive interaction. The intramolecular interactions were eliminated in order to clearly reveal the intermolecular noncovalent interaction between the adsorbate molecules and the zeolite framework. The functions RDG and $sign(\lambda_2)\rho$ were calculated with the Multiwfn software.[43]

Acknowledgements

This work was supported by the National Natural Science Foundation of China (22022202, 21991090, 21991092, 21972142, 91745109, 21703239), LiaoNing Revitalization Talents Program (XLYC1807227), the Youth Innovation Promotion Association of the Chinese Academy of Sciences (2014165), the Key Research Program of Frontier Sciences, Chinese Academy of Sciences (QYZDY-SSW-JSC024), International Partnership Program of Chinese Academy of Sciences (121421KYSB20180007).

Conflict of Interest

The authors declare no conflict of interest.

Keywords: molecular sieve · adsorption · confinement effect · solid-state NMR · theoretical calculation

- [1] M. Dusselier, M. E. Davis, Chem. Rev. 2018, 118, 5265-5329.
- [2] M. Moliner, C. Martínez, A. Corma, Chem. Mater. 2014, 26, 246-258.
- [3] M. Moliner, C. Martínez, A. Corma, Angew. Chem. Int. Ed. 2015, 54, 3560-3579; Angew. Chem. 2015, 127, 3630-3649.
- [4] P. Tian, Y. X. Wei, M. Ye, Z. M. Liu, ACS Catal. 2015, 5, 1922–1938.
- [5] J. A. Dumesic, G. W. Huber, M. Boudart, In Handbook of Heterogeneous Catalysis (Eds: G. Ertl, H. Knözinger, F. Schüth, J. Weitkamp) Wiley-VCH, Weinheim, 2008, pp. 1-15.
- [6] W. E. Farneth, R. J. Gorte, Chem. Rev. 1995, 95, 615–635.
- [7] A. M. Zheng, S. H. Li, S. B. Liu, F. Deng, Acc. Chem. Res. 2016, 49, 655-663.
- [8] G. Sastre, A. Corma, J. Mol. Catal. A: Chem 2009, 305, 3-7.
- [9] A. Bhan, E. Iglesia, Acc. Chem. Res. 2008, 41, 559-567.
- [10] Y. C. Zhi, H. Shi, L. Y. Mu, Y. Liu, D. H. Mei, D. M. Camaioni, J. A. Lercher, J. Am. Chem. Soc. 2015, 137, 15781-15794.
- [11] G. N. Kalantzopoulos, F. Lundvall, K. Thorshaug, A. Lind, P. Vajeeston, I. Dovgaliuk, B. Arstad, D. S. Wragg, H. Fjellvåg, Chem. Mater. 2020, 32, 1495-1505.
- [12] M. Hunger, Catal. Rev. Sci. Eng. 1997, 39, 345–393.
- [13] A. M. Zheng, S. J. Huang, S. B. Liu, F. Deng, Phys. Chem. Chem. Phys. **2011**. 13. 14889–14901.
- [14] J. L. Bonardet, A. Gedeon, M. A. Springuel-Huet, J. Fraissard, in Molecular Sieves, vol. 5 (Eds: H. G. Karge, J. Weitkamp) Springer, Berlin, Heidelberg. 2006, pp. 164-223.
- [15] W. Wang, M. Hunger, Acc. Chem. Res. 2008, 41, 895–904.
- [16] S. T. Xu, Y. C. Zhi, J. F. Han, W. N. Zhang, X. Q. Wu, T. T. Sun, Y. X. Wei, Z. M. Liu, Adv. Catal. 2017, 61, 37-122.
- [17] L. X. Liang, F. Deng, G. J. Hou, Chin. J. Magn. Reson. 2020, 37, 1-15.
- [18] L. A. Clark, M. Sierka, J. Sauer, J. Am. Chem. Soc. 2004, 126, 936-947.
- [19] H. J. Fang, A. M. Zheng, Y. Y. Chu, F. Deng, J. Phys. Chem. C 2010, 114, 12711-12718.
- [20] Z. J. Zhang, D. X. Li, C. Luo, R. C. Qiu, Z. W. Deng, H. L. Zhang Chin. J. Maan, Reson, 2020, 37, 67-75.
- [21] P. Tian, X. Su, Y. X. Wang, Q. H. Xia, Y. Zhang, D. Fan, S. H. Meng, Z. M. Liu, Chem. Mater. 2011, 23, 1406-1413.
- [22] J. Z. Li, Y. X. Wei, J. R. Chen, P. Tian, X. Su, S. T. Xu, Y. Qi, Q. Y. Wang, Y. Zhou, Y. L. He, Z. M. Liu, J. Am. Chem. Soc. 2012, 134, 836-839.
- [23] X. Su, P. Tian, D. Fan, Q. H. Xia, Y. Yang, S. T. Xu, L. Zhang, Y. Zhang, D. H. Wang, Z. M. Liu, ChemSusChem 2013, 6, 911-918.
- [24] F. Haase, J. Sauer, J. Am. Chem. Soc. 1995, 117, 3780-3789.
- [25] M. Hunger, T. Horvath, J. Am. Chem. Soc. 1996, 118, 12302–12308.
- [26] R. Shah, J. D. Gale, M. C. Payne, J. Phys. Chem. 1996, 100, 11688–11697.
- [27] M. W. Anderson, P. J. Barrie, J. Klinowski, J. Phys. Chem. 1991, 95, 235-239.
- [28] W. Wang, M. Seiler, M. Hunger, J. Phys. Chem. B 2001, 105, 12553-12558.
- [29] W. G. Song, J. F. Haw, J. B. Nicholas, C. S. Heneghan, J. Am. Chem. Soc. **2000**, *122*, 10726–10727.
- [30] N. N. Yan, L. Wang, X. N. Liu, P. F. Wu, T. T. Sun, S. T. Xu, J. F. Han, P. Guo, P. Tian, Z. M. Liu, J. Mater. Chem. A 2018, 6, 24186–24193.
- [31] N. N. Yan, C. Ma, Y. Cao, X. N. Liu, L. Cao, P. Guo, P. Tian, Z. M. Liu, Small 2020, 16, 33.
- [32] J. L. Bonardet, J. Fraissard, A. Gedeon, M. A. Springuel-Huet, Catal. Rev. Sci. Eng. 1999, 41, 115-225.
- [33] J. Demarquay, J. Fraissard, Chem. Phys. Lett. 1987, 136, 314-318.
- [34] A. M. Zheng, S. J. Huang, W. H. Chen, P. H. Wu, H. L. Zhang, H. K. Lee, L. C. de Menorval, F. Deng, S. B. Liu, J. Phys. Chem. A 2008, 112, 7349-7356.
- [35] U. Eichler, M. Brandle, J. Sauer, J. Phys. Chem. B 1997, 101, 10035–10050.
- [36] M. J. Janik, J. Macht, E. Iglesia, M. Neurock, J. Phys. Chem. C 2009, 113, 1872-1885.
- [37] X. Su, P. Tian, J. Li, Y. Zhang, S. Meng, Y. He, D. Fan, Z. Liu, Microporous Mesoporous Mater. 2011, 144, 113-119.
- [38] M. Svensson, S. Humbel, R. D. J. Froese, T. Matsubara, S. Sieber, K. Morokuma, J. Phys. Chem. 1996, 100, 19357-19363.
- [39] W. N. Zhang, J. R. Chen, S. T. Xu, Y. Y. Chu, Y. X. Wei, Y. C. Zhi, J. D. Huang, A. M. Zheng, X. Q. Wu, X. J. Meng, F. S. Xiao, F. Deng, Z. M. Liu, ACS Catal. 2018, 8, 10950-10963.
- [40] J. D. Chai, M. Head-Gordon, Phys. Chem. Chem. Phys. 2008, 10, 6615-6620.
- [41] M. J. Frisch, G. W. Trucks, H. B. Schlegel, G. E. Scuseria, M. A. Robb, J. R. Cheeseman, G. Scalmani, V. Barone, B. Mennucci, G. A. Petersson, H. Nakatsuji, M. Caricato, X. Li, H. P. Hratchian, A. F. Izmaylov, J. Bloino, G. Zheng, J. L. Sonnenberg, M. Hada, M. Ehara, K. Toyota, R. Fukuda, J. Hasegawa, M. Ishida, T. Nakajima, Y. Honda, O. Kitao, H. Nakai, T. Vreven,

1304

Communications doi.org/10.1002/cctc.202001682

ChemCatChem

ChemCatChem 2021, 13, 1299-1305



J. A. Montgomery, J. E. Peralta, F. Ogliaro, M. Bearpark, J. J. Heyd, E. Brothers, K. N. Kudin, V. N. Staroverov, R. Kobayashi, J. Normand, K. Raghavachari, A. Rendell, J. C. Burant, S. S. Iyengar, J. Tomasi, M. Cossi, N. Rega, J. M. Millam, M. Klene, J. E. Knox, J. B. Cross, V. Bakken, C. Adamo, J. Jaramillo, R. Gomperts, R. E. Stratmann, O. Yazyev, A. J. Austin, R. Cammi, C. Pomelli, J. W. Ochterski, R. L. Martin, K. Morokuma, V. G. Zakrzewski, G. A. Voth, P. Salvador, J. J. Dannenberg, S. Dapprich, A. D. Daniels, O. Farkas, J. B. Foresman, J. V. Ortiz, J. Cioslowski, D. J. Fox, *Gaussian 09*, revision B.01, **2010**, Gaussian, Inc.: Wallingford, CT.

[42] E. R. Johnson, S. Keinan, P. Mori-Sanchez, J. Contreras-Garcia, A. J. Cohen, W. T. Yang, J. Am. Chem. Soc. 2010, 132, 6498–6506.

[43] T. Lu, F. W. Chen, J. Comput. Chem. 2012, 33, 580-592.

Manuscript received: October 15, 2020 Revised manuscript received: December 11, 2020 Accepted manuscript online: December 14, 2020 Version of record online: January 27, 2021